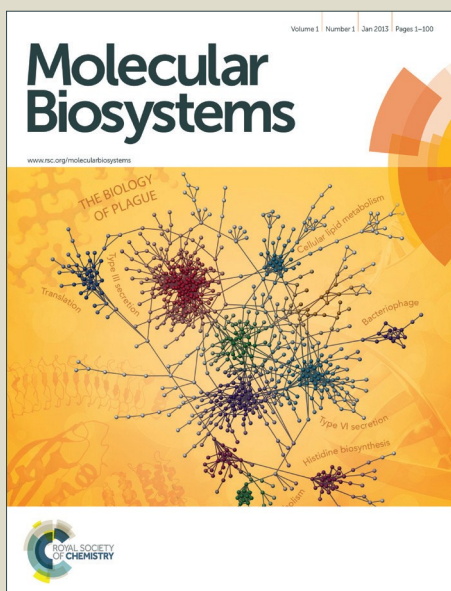


Molecular BioSystems

Accepted Manuscript



This is an *Accepted Manuscript*, which has been through the Royal Society of Chemistry peer review process and has been accepted for publication.

Accepted Manuscripts are published online shortly after acceptance, before technical editing, formatting and proof reading. Using this free service, authors can make their results available to the community, in citable form, before we publish the edited article. We will replace this *Accepted Manuscript* with the edited and formatted *Advance Article* as soon as it is available.

You can find more information about *Accepted Manuscripts* in the [Information for Authors](#).

Please note that technical editing may introduce minor changes to the text and/or graphics, which may alter content. The journal's standard [Terms & Conditions](#) and the [Ethical guidelines](#) still apply. In no event shall the Royal Society of Chemistry be held responsible for any errors or omissions in this *Accepted Manuscript* or any consequences arising from the use of any information it contains.



www.rsc.org/molecularbiosystems

Spectroscopic evidence for the role of a site of the di-iron catalytic center of ferritins in tuning the kinetics of Fe(II) oxidation

Kourosch Honarmand Ebrahimi^{¶§*}, Eckhard Bill[†], Peter-Leon Hagedoorn[¶], Wilfred R. Hagen[¶]

[¶]Department of Biotechnology, Delft University of Technology, Van der Maasweg 9, 2629 HZ Delft, The Netherlands. [†]Max Planck Institute for Chemical Energy Conversion (MPI-CEC), Stiftstrasse 34-36, D-45470 Mülheim, Germany.

[§]Present address: Department of Chemistry, University of Oxford, South Parks Road, Oxford, OX1 3QR,

To whom correspondence should be addressed: Kourosch H. Ebrahimi, Department of Chemistry, University of Oxford, South Parks Road, Oxford, OX1 3QR, Tel: +44(0)1865 272649, Email: kourosch.honarmandebrahimi@chem.ox.ac.uk

Keywords: Ferritin, Unity, Fe(II) oxidation, Iron metabolism, ferroxidase

1 Abstract

2 Ferritin is a nanocage protein made of 24 subunits. Its major role is to manage intracellular concentrations
3 of free Fe(II) and Fe(III) ions, which is pivotal for iron homeostasis across all Domains of life. This
4 function of the protein is regulated by a conserved di-iron catalytic center and has been the subject of
5 extensive studies over the past 50 years. Yet, it has not been fully understood how Fe(II) is oxidized in the
6 di-iron catalytic center and it is not known why eukaryotic and microbial ferritins oxidize Fe(II) with
7 different kinetics. In an attempt to obtain new insight into the mechanism of Fe(II) oxidation and
8 understand the origin of the observed differences in the catalysis of Fe(II) oxidation among ferritins we
9 studied and compared the mechanism of Fe(II) oxidation in the eukaryotic human H-type ferritin (HuHF)
10 and the archaeal ferritin from *Pyrococcus furiosus* (Pfftn). The results show that the spectroscopic
11 characteristics of the intermediate of Fe(II) oxidation and the Fe(III)-products are the same in these two
12 ferritins supporting the proposal of unity in the mechanism of Fe(II) oxidation among eukaryotic and
13 microbial ferritins. Moreover, we observed that a site in the di-iron catalytic center controls distribution of
14 Fe(II) among subunits of HuHF and of Pfftn differently. This observation explains the reported
15 differences between HuHF and Pfftn in the kinetics of Fe(II) oxidation and the amount of O₂ consumed
16 per Fe(II) oxidized. These results provide a fresh understanding of the mechanism of Fe(II) oxidation by
17 ferritins.

18

1 Introduction

2 The 24-meric ferritin (Figure 1A) has a nanocage-like structure, which has found a wide range of
3 applications¹⁻³ in nanotechnology, biocatalysis, and medicine. The major physiological role of ferritin is
4 to manage intracellular concentrations of free Fe(II) and Fe(III) ions. This key function of protein depends
5 on the oxidation of Fe(II) to Fe(III) in the di-iron center of the catalytically active subunits. This unique
6 di-iron center is known as the ferroxidase center (Sites A and B in Figure 1B). A third transient site,
7 known as site C, has been identified as a gateway to the ferroxidase center in eukaryotic⁴⁻⁶, bacterial^{7, 8},
8 and archaeal ferritins^{1, 4} (Figures 1B-C). The overall mechanism of Fe(III) storage in ferritins can be
9 defined as: (i) Fe(II) entry and access to the ferroxidase center, (ii) Fe(II) oxidation at the ferroxidase
10 center, and (iii) Fe(III) storage in the central cavity. The Fe(II) ions reach the ferroxidase center through
11 the protein shell^{5, 9-12}. Oxidation of Fe(II) occurs in the ferroxidase center and site C^{1, 13}. The mechanism
12 of Fe(II) oxidation is not fully understood. Previous studies have led to the proposal of different models
13 for the mechanism of Fe(II) oxidation in eukaryotic and microbial ferritins¹⁴⁻¹⁶. While for eukaryotic
14 human H-type ferritin (HuHF)¹⁷ and bullfrog M-type ferritin (BfMF)¹⁸ it is proposed that under single
15 turnover conditions, i.e. addition of Fe(II) per subunit ≤ 2 , two Fe(II) are simultaneously oxidized in
16 each ferroxidase center, for human mitochondrial ferritin it is proposed that less ferroxidase centers are
17 active and Fe(II) might be oxidized by Fe(III) mineral core¹⁹. For BfMF¹⁸ and BfHF²⁰ similar Mössbauer
18 data obtained during the catalytic reaction have been interpreted differently to reflect different
19 mechanisms of Fe(II) oxidation. It has been proposed that in BfMF Fe(II) is oxidized via a peroxodiferric
20 intermediate, while in BfHF Fe(II) is oxidized via a tyrosine radical. On the other hand it is believed that
21 in *E.coli* ferritin A (EcFtnA) three Fe(II) are simultaneously oxidized in sites A, B, and C²¹. On the basis
22 of these data the diversity view has emerged claiming that the mechanism of Fe(II) oxidation and Fe(III)
23 storage varies among ferritins^{14, 15, 22}. In contrast our studies of the hyperthermophilic archaeal ferritin
24 from *Pyrococcus furiosus* (PfFtn) and HuHF in comparison showed that in eukaryotic and microbial

1 ferritins Fe(III) stays metastably in the ferroxidase center and is displaced by the incoming Fe(II)⁴. This
2 displacement of Fe(III) by Fe(II) was proposed to be the basis of a common mechanism of Fe(III)-storage
3 among ferritins^{1, 4, 23}. Based on these data and a re-evaluation of previous studies on other ferritins we put
4 forward the proposal of unity in the biochemistry of ferritins¹. We proposed that although variations in the
5 amino acid sequences of ferritins exist the chemistry of Fe(II) oxidation and Fe(III) storage is the same
6 among eukaryotic and microbial ferritins¹.

7 In our previous studies using HuHF and PfFtn we observed that the kinetics of Fe(II) oxidation were
8 different¹³, but the progress curves of Fe(II) oxidation could be simulated using a common model¹³. These
9 observations prompted us to further investigate the intermediates of Fe(II) oxidation in these two ferritins.
10 We applied freeze quench electron paramagnetic resonance (EPR) and Mössbauer spectroscopy together
11 with UV-visible stopped-flow spectroscopy. HuHF and PfFtn were compared because they consist of 24
12 catalytically active subunits and because they are from two distinct Domains of life and should serve as a
13 good model to test the diversity view against the unity view. The results strongly suggest that Fe(II)
14 oxidation in both HuHF and PfFtn proceeds via the same peroxodiferric intermediate and results in the
15 same Fe(III) products in support of the proposal of unity in the biochemistry of ferritins. Our data further
16 provide new insight into the initial step of catalysis of Fe(II)-oxidation, i.e. Fe(II) binding to the catalytic
17 sites, and shed light on a possible explanation for the observed differences in the kinetics of Fe(II)
18 oxidation among eukaryotic and microbial ferritins.

19

20 **Experimental procedure.**

21 Details of chemicals, protein expression and purification, UV-visible stopped-flow experiments, and
22 statistical analysis of Mössbauer data are included in the Supplementary Information file.

1 *Choosing the time points for freeze quench to trap the Fe(II) oxidation reaction intermediates of ferritin.*
2 In ferritin the Fe(II) is substrate and the Fe(III) is product and during catalysis of Fe(II) oxidation
3 different species such as Fe(II) substrate, Fe(III) intermediates, and Fe(III) products can coexist. As a
4 consequence simulation of Mössbauer data to characterize Fe(III) intermediates will be complex if large
5 amounts of different Fe(III) products are present. To decrease this complexity and to obtain new insight
6 about various different intermediates, the reaction was quenched at three time points. (i) Before addition
7 of molecular oxygen ($t=0$) at which all the iron should be Fe(II). (ii) A time point after addition of
8 molecular oxygen at which the absorbance of the peroxodiferric intermediate was close to its maximum in
9 PfFtn and HuHF (see below). The same time point was chosen for HuHF and PfFtn for proper
10 comparison of the intermediates; (iii) At a time point when all of the Fe(II) was converted to Fe(III)
11 products and no further change in the absorbance spectrum from 300-700 nm was observed.

12 *Preparation of EPR and Mössbauer samples before addition of dioxygen ($t=0$ s).* The $^{57}\text{Fe(II)}$ or $^{\text{NAT}}\text{Fe(II)}$
13 (natural abundance Fe(II)) solution was prepared in acidic Milli Q. water, i.e. $\text{pH} \leq 2$. PfFtn or HuHF was
14 prepared in 1M MOPS buffer, 200 mM NaCl, pH 7.0. This concentration of buffer was chosen to
15 minimize any change in the pH after mixing protein with the acidic Fe(II) solution in 1:1 ratio. Final
16 concentration of buffer was 500 mM MOPS, 100 mM NaCl, pH 7.0. To prepare the samples before
17 reaction of Fe(II)-bound ferritin with dioxygen (samples labelled $t=0$ s) anaerobic solutions of Fe(II) and
18 ferritin were mixed (1:1 ratio) in an anaerobic glove box (Coy Laboratories). 250 μl or 500 μl of the
19 solution was then transferred to an EPR tube or a customized Mössbauer sample tube in the glove box,
20 EPR and Mössbauer tubes were tightly closed. Subsequently, they were transferred outside the glove box
21 and immediately frozen in liquid nitrogen.

22 *Preparation of EPR and Mössbauer samples 0.7 s quenched after reaction with dioxygen.* PfFtn or HuHF
23 was in 1M MOPS buffer, 200 mM NaCl, pH 7.0. The Fe(II) solution should have a pH of less than 2 to

1 prevent autoxidation of Fe(II) under dioxygen saturation conditions (Supplementary Figure 1). Ferritin
2 and Fe(II) solutions were kept in different gas tight bottles and were purged with pure dioxygen gas for
3 circa 10 minutes to reach oxygen saturation conditions. The solutions were then immediately used for
4 rapid freeze quench experiments. Freeze-quench samples were prepared by connecting an in-house build
5 T-mixer cell to the stopped-flow instrument as explained previously¹³. One syringe of the stopped-flow
6 instrument was filled with ferritin and the other syringe was filled with Fe(II) solution, each syringe circa
7 300 μl . The solutions were then rapidly mixed through the T-mixer cell by applying 9 bar pressure behind
8 each syringe. This setup was used because the time scale of the reaction in Pfftn at room temperature is
9 much longer than the millisecond time scale usually associated with rapid freeze-quench techniques. To
10 apply this setup to quench the reaction of Pfftn and HuHF with circa 2 Fe(II) per ferritin subunit, using
11 stopped-flow spectroscopy we determined the optimum temperature at which the absorbance of the
12 peroxodiferric intermediate reached its maximum circa 0.7 s after mixing. This time was chosen because
13 it was the dead time of mixing and freezing for our freeze quench setup, as determined using the
14 myoglobin-azide reaction¹³. The optimum temperature for HuHF was 10 °C and for Pfftn it was 47 °C.
15 Increasing the temperature to higher values for Pfftn was not possible due to instrumental limitations.
16 The outflow from the mixer was directly injected into customized EPR or Mössbauer tubes, which were
17 cooled with and kept in liquid nitrogen by using an extension tubing of 10 cm length. This time is quoted
18 in the text as the shortest quenching time of the reaction for EPR or Mössbauer spectroscopy. To quench
19 the reaction after a long time, circa 1-5 minutes, the solutions were injected into room temperature EPR or
20 Mössbauer tubes. The samples were frozen by immersing in liquid nitrogen 300 s (Pfftn) after incubation
21 at 47 °C, or 60 s (HuHF) after incubation at 10 °C. For Mössbauer spectroscopy the final concentrations
22 of Pfftn and HuHF, after 1:1 mixing with ⁵⁷Fe(II) solution, were 45 μM (24-mer) and 55 μM (24-mer)
23 respectively. The volume of the Mössbauer samples was either circa 500 μl or circa 250 μl . For EPR
24 spectroscopy the final concentration of Pfftn was 45 μM (24-mer) or 4.4 μM (24-mer), and that of HuHF

1 was 55 μM (24-mer) or 5.5 μM (24-mer). For EPR and Mössbauer samples the final concentration of
2 $^{\text{NAT}}\text{Fe}$ or ^{57}Fe was set to achieve a total loading of 50 Fe(II) per ferritin 24-mer, this was done to make
3 sure that two Fe(II) per ferritin subunit were added. The solubility of dioxygen at 10 °C is circa 1.71 mM
4 and at circa 47 °C is about 0.96 mM. Because under single-turnover conditions in Pfftn the stoichiometry
5 of Fe(II) oxidized per dioxygen is circa 3 and in HuHF it is circa 2.5¹³, enough dioxygen for a single
6 turnover of enzyme must be present under our experimental conditions. Pfftn and Fe(II) solutions were
7 preheated to 47 °C for 1 minute before 1:1 mixing, HuHF and Fe(II) solutions were cooled at 10 °C for 1
8 minute before 1:1 mixing. The pressure of the stopped-flow N₂ gas, which is used for shooting the protein
9 and Fe(II) solutions for rapid mixing, was 9 bar.

10 *Electron paramagnetic resonance (EPR) spectroscopy.* X-band EPR measurements were performed using
11 a Bruker ECS-106 EPR spectrometer. EPR conditions were: microwave power 0.127-201 mW;
12 modulation frequency 100 kHz; modulation amplitude, 12.7 or 4.02 Gauss; Temperature 6.4-30 K. EPR
13 spectra were analyzed using programs described in²⁴.

14 *Mössbauer spectroscopy.* Mössbauer spectra were recorded on a conventional spectrometer with
15 alternating constant acceleration of the γ -source. The minimum experimental line width was 0.24 mms^{-1}
16 (full width at half-height). The sample temperature was maintained constant either in an Oxford
17 Instruments Variox or an Oxford Instruments Mössbauer-Spectromag cryostat with a split-pair magnet
18 system. Measurements were performed at 80 K. The γ -source ($^{57}\text{Co}/\text{Rh}$, 1.8 GBq) was kept at room
19 temperature. By using a re-entrant bore tube the γ -source could be positioned inside the gap of the magnet
20 coils at a position of zero field. Isomer shifts are quoted relative to iron metal at 300K.

21

22 **Results.**

1 **Fe(II) distribution among three sites is different in HuHF and Pfftn.** The first step in catalysis of
2 Fe(II) oxidation is binding of the Fe(II) ions to the metal ion binding sites in each subunit. As discussed in
3 the introduction three Fe(II) binding sites exist in different eukaryotic and microbial ferritins^{1,6}, i.e. sites
4 A and B of the ferroxidase center and site C close to this center. We have showed previously that Fe(II)
5 distributes among these sites⁴. However, we could not determine the Fe(II) occupation of each site to
6 define the amount of different types of Fe(II)-occupied subunits under single-turnover conditions, i.e.
7 addition of circa 2 Fe(II) per ferritin subunit. This knowledge is essential for understanding the
8 mechanism of Fe(II) oxidation. To determine the Fe(II) occupation of each site before addition of
9 dioxygen we used Mössbauer spectroscopy and combined the results with knowledge of the binding
10 affinity of each site for Fe(II), which we had determined in a previous study using detailed isothermal
11 titration calorimetry experiments under anaerobic conditions⁴ (Supplementary Table 1). Two Fe(II) ions
12 per ferritin subunit were added to apo-HuHF or apo-Pfftn under anaerobic conditions. Simulation of the
13 Mössbauer spectra required a model of three distinct Fe(II) doublets (Figure 2A and Supplementary
14 Figures 2-3). We attribute these doublets to the three individual sites, i.e. sites A, B, and C (Table 1), in
15 agreement with the observation of three sites with different coordination environments using X-ray
16 crystallography in various ferritins¹ including Pfftn²⁵ and HuHF⁶. These observations are inconsistent
17 with the possibility that only one or two sites might exist. Furthermore, the hypothesis that two of the
18 Fe(II) doublets might be assigned to a single site with alternative coordination ligands can also be ruled
19 out based on our Mössbauer data. The sum of the amount of any combination of two different doublets
20 exceeds the total number of site A, or B, or C present in a ferritin 24-mer. For example the second and the
21 third doublets in Pfftn together account for circa 60% of the Fe(II)-added. This means circa 29 Fe(II) per
22 ferritin 24-mer. Because there are only 24 sites A, or B, or C per ferritin 24-mer available, the second and
23 the third doublets in Pfftn cannot be assigned to the same site with alternative coordination ligands. The
24 Mössbauer parameters of the first doublet in HuHF and in Pfftn are very close (Table 1). Because the

1 Mössbauer parameters of Fe(II) in the absence of dioxygen are mainly affected by its amino acid
2 coordinating residues, the coordination environments of the Fe(II) associated with the doublet in HuHF
3 and Pfftn should be the same. The available structural data¹ shows exactly the same coordination
4 environment for site A in Pfftn and HuHF (Figure 2B), but not for sites B and C. Consequently, we
5 attribute the first Fe(II) doublet to the Fe(II) in site A of the ferroxidase center. In Pfftn the second
6 (purple trace in figure 2A) and the third (orange trace in figure 2A) Fe(II) doublets have 40% and 19%
7 abundance respectively (Table 1). In Pfftn as we reported previously⁴ the affinity of site B for Fe(II), i.e.
8 $(5.5 \pm 1.0) \times 10^4 \text{ M}^{-1}$, is 50-fold higher than that of site C, i.e. $(1.0 \pm 0.3) \times 10^3 \text{ M}^{-1}$ (Supplementary Table
9 1). Therefore, in Pfftn the doublet with 40% abundance is attributed to site B and the doublet with 19%
10 abundance is attributed to site C. In HuHF the abundances of the second (purple trace in figure 2A) and
11 the third (orange trace in figure 2A) Fe(II) doublets are within experimental error the same (Table 1). This
12 is consistent with the observation that sites B and C in HuHF have the same affinity for Fe(II) ions
13 (Supplementary Table 1)⁴. The exact assignment of the second and the third Fe(II) doublets in HuHF to
14 sites B and C was not possible.

15

16 **Mössbauer spectroscopy reveals different forms of Fe(II)-filled subunits.** For distribution of Fe(II)
17 among three binding sites, statistically seven Fe(II)-occupation scenarios for subunits can be imagined:
18 subunits with Fe(II)-occupied site A only ($A^{\text{II}}B^0C^0$), or site B only ($A^0B^{\text{II}}C^0$), or site C only ($A^0B^0C^{\text{II}}$),
19 subunits with Fe(II)-occupied sites A and B ($A^{\text{II}}B^{\text{II}}C^0$), subunits with Fe(II)-occupied sites A and C
20 ($A^{\text{II}}B^0C^{\text{II}}$), subunits with Fe(II)-occupied sites B and C ($A^0B^{\text{II}}C^{\text{II}}$), and subunits with Fe(II)-occupied sites
21 A, B, and C ($A^{\text{II}}B^{\text{II}}C^{\text{II}}$). Site A has the highest affinity for Fe(II) as determined for different ferritins^{4, 26}
22 (Supplementary Table 1). Thus, site A should first be occupied with Fe(II). Occupation of site A will be
23 followed by Fe(II) binding to sites B and C, possibly in a cooperative fashion. Therefore, among the

1 above seven Fe(II)-occupation scenarios four predominate (Figure 3): ($A^{II}B^{II}C^0$) subunits with Fe(II)-
 2 occupied sites A and B but empty site C; ($A^{II}B^{II}C^{II}$) subunits with Fe(II)-occupied sites A, B, and C;
 3 ($A^{II}B^0C^{II}$) subunits with Fe(II)-occupied sites A and C but empty site B; and ($A^{II}B^0C^0$) subunits with
 4 Fe(II)-occupied site A only. To estimate the percentage of each subunit type per ferritin 24-mer using the
 5 results of Mössbauer spectroscopy we define three variables:

$$6 \quad X = \frac{\%(A^{II}B^0C^0) + \%(A^{II}B^{II}C^0) + \%(A^{II}B^0C^{II}) + \%(A^{II}B^{II}C^{II})}{100} \quad (1)$$

$$7 \quad Y = \frac{\%(A^{II}B^{II}C^0) + \%(A^{II}B^{II}C^{II})}{100} \quad (2)$$

$$8 \quad Z = \frac{\%(A^{II}B^0C^{II}) + \%(A^{II}B^0C^0)}{100} = X - Y \quad (3)$$

9 in which X is the sum of the percentages of all subunit types divided by 100, Y is the sum of the
 10 percentages of subunits with sites A and B occupied divided by 100, and Z is the percentages of subunits
 11 with site B empty divided by 100. As we discussed above, site A is first occupied with Fe(II) and
 12 subsequently sites B and C are filled. Thus, ‘X’ or ‘Y’ are a factor of the amount of Fe(II) added per
 13 subunit and the percentage of Fe(II) assigned to site A or B respectively. Accordingly we may write:

$$14 \quad X = \frac{\left(\frac{n \times \% \text{ Fe(II) in site A}}{24 \text{ subunits}} \right)}{100} \quad (4)$$

$$15 \quad Y = \frac{\left(\frac{n \times \% \text{ Fe(II) in site B}}{24 \text{ subunits}} \right)}{100} \quad (5)$$

16 In which “n” is the amount of Fe(II) added per ferritin 24-mer for a single turnover experiment. In our
 17 experiments “n” was 50 Fe(II) per ferritin 24-mer. % Fe(II) in site A or B is the percentage of Fe(II)
 18 doublet assigned to site A or B based on the results of Mössbauer spectroscopy for samples before
 19 addition of dioxygen (Table 1). X and Y are calculated using equations 4 and 5, and subsequently the

1 percentage of four different Fe(II)-occupied subunit types (Figure 3) was found using the following
 2 equations (see supplementary materials for details):

$$3 \quad \%A^{II}B^0C^{II} = \frac{n \times \%Fe(II) \text{ in site C}}{24 \text{ subunits}} \times (Z) \quad (6)$$

$$4 \quad \%A^{II}B^{II}C^{II} = \frac{n \times (\%Fe(II) \text{ in site C} - \% \text{ of } Fe(II) \text{ in site C of } A^{II}B^0C^{II})}{24 \text{ subunits}} \times Y \quad (7)$$

$$5 \quad \%A^{II}B^{II}C^0 = (Y \times 100) - \%A^{II}B^{II}C^{II} \quad (8)$$

$$6 \quad \%A^{II}B^0C^0 = (Z \times 100) - \%A^{II}B^0C^{II} \quad (9)$$

7 in which % Fe(II) in site B or C is obtained from the results of Mössbauer spectroscopy for samples
 8 before addition of dioxygen. Using equations 6-9 we found that the percentage of ($A^{II}B^{II}C^0$) subunits in
 9 Pfftn and HuHF is circa 52% and 42% respectively and that of ($A^{II}B^{II}C^{II}$) subunits in Pfftn and HuHF is
 10 32% and 14% respectively (Figure 3). The percentages of ($A^{II}B^0C^{II}$) and ($A^{II}B^0C^0$) subunits in Pfftn is
 11 circa 1% each, while in HuHF they are circa 13% and 12% respectively (Figure 3). Because in some
 12 subunits, i.e. ($A^{II}B^{II}C^{II}$) subunits, three sites are occupied upon addition of circa 2 Fe(II) per subunit and
 13 because the percentage of ($A^{II}B^{II}C^{II}$) subunits is more than that of ($A^{II}B^0C^0$) subunits, in total only circa
 14 80-90% of the subunits is observed to be occupied. Moreover, it should be noted that although we could
 15 not specifically assign the second and the third Fe(II) doublets in HuHF to sites B and C, because their
 16 amounts are within experimental error the same the results obtained using our statistical model are valid
 17 for HuHF. Our observations regarding the distribution of Fe(II) are consistent with a possible positive
 18 cooperativity among subunits and among three binding sites, i.e. binding of Fe(II) to site A in one subunit
 19 induces binding of Fe(II) to site A in a nearby subunit and to sites B and C. Indeed kinetics of Fe(II)
 20 oxidation have shown positive cooperativity in eukaryotic and microbial ferritins due to a yet to be
 21 identified mechanism^{13,27}.

1

2 **The same peroxodiferric intermediate is formed in HuHF and Pfftn.** An intermediate with visible
3 absorbance between 500-800 nm and centered at a different wavelength in different ferritins^{1, 7, 19, 28-30} has
4 been reported during catalysis of Fe(II) oxidation. For example the progress curves of this intermediate in
5 HuHF (650 nm) and Pfftn (620 nm) are shown in figure 4A and 4B respectively. We applied freeze
6 quench EPR and Mössbauer spectroscopy to obtain molecular insight into the origin of this intermediate
7 in these ferritins. The reaction of HuHF or Pfftn containing circa 2 ⁵⁷Fe(II) per ferritin subunit was
8 quenched 0.7 s after addition of dioxygen to compare the intermediates at the same freezing time. This
9 time was chosen because the absorbance of the Fe(III) intermediate species reached its maximum in
10 HuHF (Figure 4A) and was close to maximum in Pfftn (Figure 4B) (Methods). Simulation of the
11 Mössbauer spectrum of Pfftn suggested the presence of one Fe(II) and two Fe(III) doublets (Figure 4C
12 and Supplementary Figure 4), and that of HuHF suggested the presence of two Fe(II) and three Fe(III)
13 doublets (Figure 4C and Supplementary Figure 5). The ratio of the two major Fe(III) doublets in HuHF
14 and Pfftn (green and purple traces in figure 4C) was constrained to 1:1 abundance (Table 2). This was
15 done because EPR spectroscopy implied that the majority of the Fe(III) ions should be in a spin-coupled
16 diferric intermediate with S=0 ground state (EPR silent): EPR spectroscopy showed only negligible spin
17 concentration of the total Fe(II) added as a mononuclear Fe(III) species or a [Fe(II)-Fe(III)] mixed
18 valence cluster⁴ (Supplementary Table 2). The Mössbauer parameters of the diferric intermediate in
19 HuHF are similar to those of the diferric intermediate in Pfftn (Table 2). This implies that the molecular
20 structure of the diferric intermediate in HuHF and Pfftn is the same. These parameters are compared to
21 those of the various peroxodiferric intermediate species in model compounds³¹⁻³⁷ and in dioxygen
22 activating enzymes³⁸⁻⁴¹ (Table 3). From table 3 one can observe that the Mössbauer parameters assigned
23 to the μ -1,2-peroxodiferric binding mode span over a wide range, but for the majority of cases, at least
24 one of the reported values for the ΔE_Q is above 1.4 (mm/s) (Table 3). On the other hand for the cases in

1 which the peroxo species is assigned to η^2 -O₂ binding mode a ΔE_Q of less than 0.8 (mm/s) is reported.
2 Similar to the η^2 -O₂ binding mode of the peroxo, in PfFtn and HuHF one of the ΔE_Q of the peroxodiferric
3 intermediate is less than 0.8 (mm/s) (Table 3). Because EPR spectroscopy showed that two Fe(III) in the
4 ferroxidase center are antiferromagnetically coupled, we propose that the peroxodiferric intermediate in
5 HuHF and PfFtn has a μ - η^1 : η^2 core structure. Further investigations with e.g. resonance Raman or
6 EXAFS spectroscopy may be used to corroborate this proposal. It should be noted that the Mössbauer
7 parameters we found in HuHF are different from those previously reported⁴². Previous Mössbauer studies
8 with HuHF⁴² were performed at $\text{pH} \leq 6.5$, a pH value at which Fe(II) binding to the site A of the
9 ferroxidase center is known to be disrupted²⁶. Fe(II) binding under anaerobic conditions to sites A, B, and
10 C in HuHF has been observed by isothermal titration calorimetry⁴ or X-ray crystallography¹⁰ at $\text{pH} \geq 7$.

11
12 **Only in (A^{II}B^{II}C⁰) and (A^{II}B^{II}C^{II}) subunits can two Fe(II) be simultaneously oxidized.** It has been
13 previously proposed that in eukaryotic ferritins two Fe(II) together are simultaneously oxidized in each
14 ferroxidase center to form the peroxodiferric intermediate^{17, 18, 43}, while in bacterial ferritins three Fe(II),
15 two Fe(II) in the ferroxidase center together with the Fe(II) in site C, are simultaneously oxidized^{21, 44}.
16 These proposals predict that under single-turnover conditions, when the absorbance of the peroxodiferric
17 intermediate reaches its maximum, i.e. 0.7 s in our experiments, all of the Fe(II) added should have been
18 converted to the peroxodiferric intermediate or to products. Our Mössbauer data and those reported
19 previously for BfMF²⁹ and BfHF²⁰ are inconsistent with this proposal. We analysed the Mössbauer data of
20 the Fe(II) doublets before addition of dioxygen (Table 1) and those of the Fe(II)/Fe(III) doublets 0.7 s
21 after addition of dioxygen (Table 2). As discussed above the results of Mössbauer spectroscopy before
22 addition of dioxygen revealed the amounts of different forms of Fe(II)-occupied subunits for PfFtn and
23 HuHF (Figure 3). In PfFtn and HuHF 0.7 s after addition of dioxygen the amount of Fe(III) observed as

1 the peroxodiferric intermediate was circa 84% and 58% (Table 2), which represent circa 84% of subunits
2 in Pfftn and 58% of subunits in HuHF. Comparison of these values with the percentages of ($A^{II}B^{II}C^0$)
3 and ($A^{II}B^{II}C^{II}$) subunits in figure 5 shows that they are within experimental error the same as the sum of
4 the percentages of ($A^{II}B^{II}C^0$) and ($A^{II}B^{II}C^{II}$) subunits in Pfftn (84%) and in HuHF (56%) respectively.
5 These data suggest to us that both in Pfftn and in HuHF the Fe(II) ions in sites A and B of the ($A^{II}B^{II}C^0$)
6 and ($A^{II}B^{II}C^{II}$) subunits were oxidized concurrently within 0.7 s to form the peroxodiferric intermediate,
7 but the Fe(II) ions in site C of the ($A^{II}B^{II}C^{II}$) subunits or sites A and C of the ($A^{II}B^0C^0$) and ($A^{II}B^0C^{II}$)
8 subunits were not oxidized rapidly (Figure 5). Consistently, in Pfftn one Fe(II) doublet (16%) was
9 observed (Table 2) whose amount was within experimental error close to the amount of the Fe(II) doublet
10 attributed to site C (19%) under anaerobic conditions (Table 1). However, the Mössbauer parameters of
11 the Fe(II) doublet attributed to site C before (Table 1) and after (Table 2) addition of dioxygen were
12 different. The reason for this difference is not known but may suggest a change in the coordination
13 environment of site C in Pfftn upon Fe(II) oxidation in the ferroxidase center. In HuHF 0.7 s after
14 addition of dioxygen two Fe(II) doublets were observed (Table 2). The Mössbauer parameters of the first
15 Fe(II) doublet (12%) (Table 2) are the same as the Fe(II) doublet attributed to site A before addition of
16 dioxygen (Table 1). The amount of this doublet (12%) is consistent with the oxidation of Fe(II) in sites A
17 and B, and formation of the peroxodiferric intermediate in the ferroxidase center: in HuHF before
18 addition of dioxygen the amount of Fe(II) in site B was only 25-27% of the Fe(II) added. As a result upon
19 addition of dioxygen only 25-27% of the 39% Fe(II) in site A could rapidly oxidize to form the
20 peroxodiferric intermediate. Circa 12% of the Fe(II) in site A could not be oxidized rapidly. The second
21 Fe(II) doublet in HuHF (Table 2) should be the Fe(II) in site C, since this Fe(II) has not entered the
22 ferroxidase center and cannot be oxidized rapidly together with the Fe(II) in site A of the ferroxidase
23 center. In summary, the data for Pfftn and HuHF together demonstrate that only in ($A^{II}B^{II}C^0$) and
24 ($A^{II}B^{II}C^{II}$) subunits two Fe(II) are oxidized simultaneously in the ferroxidase center. In subunits in which

1 site B is not occupied, Fe(II) in site A cannot be oxidized (Figure 5). We speculate that site B might be
2 the initial dioxygen binding site. This suggestion is in line with a previous site directed mutagenesis study
3 of HuHF in which differences between sites A and B of the ferroxidase center were observed⁴⁵.
4 Replacement of a glutamate residue of each site resulted in a different response to Fe(II) oxidation. Based
5 on this observation it has been proposed that differences exist between sites A and B, and that site B is
6 possibly the initial dioxygen binding site⁴⁵.

7

8 **Site B tunes the kinetics of Fe(II) oxidation.** Progress curves of Fe(III) formation, which are typically
9 measured between 300-350 nm, have been recorded for various ferritins using stopped-flow spectroscopy
10^{6, 7, 17, 21}. Even though previous Mössbauer data showed that when the peroxodiferric intermediate has its
11 maximum absorbance not all the Fe(II) ions are oxidized^{18, 20, 29}, the progress curves have been interpreted
12 as formation of the peroxodiferric in each subunit as a sudden increase in the absorbance followed by
13 spontaneous transfer of the Fe(III) product to the internal cavity of ferritin observed as a gradual increase
14 of the absorbance in a slower phase^{17, 18, 20, 29}. UV-visible spectroscopy by itself does not provide direct
15 information on the nature of Fe(II) and Fe(III), e.g. whether the Fe(III) species are intermediates or
16 products. To properly interpret the stopped-flow UV-visible data (Figure 6) in terms of formation of
17 different Fe(III) species we used our Mössbauer data. The recorded progress curves are consistent with
18 those reported previously for HuHF^{13, 17, 30} or Pfftn^{13, 30}. The data were analyzed based on the amount of
19 doublets assigned to the Fe(II) substrate and the peroxodiferric intermediate observed 0.7 s after addition
20 of dioxygen (Table 2). Under single-turnover conditions, a two-exponential equation (Equation 10) was
21 required to obtain a fit to the data using global fit analysis:

$$22 \quad F(t) = -Me^{\left(\frac{-t}{T_1}\right)} - Ne^{\left(\frac{-t}{T_2}\right)} + M_\infty \quad (10)$$

1 in which M and N are the pre-exponential amplitude factor (the absorbance of each exponential phase),
2 T_1 and T_2 are time constants, and M_∞ is the absorbance at infinite time. The values of M, N, T_1 , T_2 , and
3 M_∞ for PfFtn and HuHF are given in table 4. In PfFtn and HuHF the ratio of the M to M_∞ was circa 80%
4 and 50% respectively. This suggests that in PfFtn circa 80% and in HuHF circa 50% of the Fe(II) added
5 was rapidly oxidized in the first phase. This is consistent with the observation of circa 84% and circa 58%
6 Fe(III) as the peroxodiferric intermediate in PfFtn and in HuHF respectively (Table 2). Thus, the fast
7 phase should present the rapid formation of the peroxodiferric intermediate in the ($A^{II}B^{II}C^0$) and
8 ($A^{II}B^{II}C^{II}$) subunits and not the Fe(III) products. Moreover, the ratio of N to M_∞ in PfFtn and HuHF was
9 circa 20% and 50% respectively. These ratios represent the percentages of Fe(II) not oxidized in the first
10 phase but oxidized in the second slow phase plus a possible small change in the absorbance due to
11 conversion of the peroxodiferric intermediate to the Fe(III) products. They are close to the percentages of
12 Fe(II) observed by Mössbauer spectroscopy in PfFtn (16%) and in HuHF (37%) 0.7 s after addition of
13 dioxygen (Table 2). Therefore, the Fe(II) that was not oxidized rapidly in the first phase was oxidized at a
14 slower rate in the second phase. These data demonstrate that the kinetics of Fe(II) oxidation are defined
15 by the amount of the peroxodiferric intermediate that can rapidly form as a result of the presence of Fe(II)
16 in site B of the ferroxidase center.

17

18 **The Fe(III)-dimer in the ferroxidase center is the major product of the Fe(II) oxidation.** After
19 complete oxidation of Fe(II), i.e. after 300 s in PfFtn and 60 s in HuHF, we recorded the presence of
20 different Fe(III)-product species in ferritins. The Mössbauer spectra of PfFtn and HuHF could be
21 simulated using a model of two Fe(III) doublets (Figure 7 and Supplementary Figures 6-7). The
22 Mössbauer parameters of these doublets were different from those of the peroxodiferric intermediate. The
23 first doublet in PfFtn and HuHF accounts for circa 42% of the Fe(III) (Table 5), which is the same as the

1 amount of Fe(II) in site A before addition of dioxygen (Table 1). Therefore, this doublet is assigned to
2 Fe(III) in site A. The second doublet accounts for 58% Fe(III) (Table 5), which is the same as the sum of
3 the Fe(II) in sites B and C before addition of dioxygen (Table 1). The Mössbauer parameters of the Fe(III)
4 products in ferritin are similar to those reported for oxo or hydroxo bridged di-iron complexes⁴⁶. This is
5 consistent with the results of EPR spectroscopy. Only circa 2-5 % of the total Fe(II) added showed up as
6 an EPR detectable ($g=4.3$) mononuclear Fe(III) species (Supplementary table 2). Because 42% of the
7 Fe(III) ions was assigned to site A, at least 42% of the Fe(III) ions should have been in site B to form the
8 antiferromagnetically coupled Fe(III)-O(H)-Fe(III) unit in the ferroxidase center, which is EPR silent.
9 This interpretation is consistent with our previous observation that after complete oxidation of Fe(II) the
10 majority of the ferroxidase centers remain occupied with two Fe(III), and the Fe(III) ions are displaced by
11 incoming new Fe(II) ions⁴. Two fates for the remaining 16% of Fe(III) can be considered: some of the
12 Fe(III) stayed in site C and was observed as mononuclear Fe(III) and some moved to the internal cavity to
13 form the Fe(III)-mineral core. Further detailed low temperature high-field Mössbauer measurements are
14 required to study the nature of the mineral core in each ferritin.

15

16 **Discussion.**

17 Because oxidation of Fe(II) by ferritin is vital for the iron homeostasis machinery of all life forms, for
18 more than half a century, this reaction has been studied intensively using ferritins from different
19 organisms. Although the quaternary structure of ferritins is highly conserved, differences exist in the
20 amino acid residues essential for the functioning of protein. A notable variation among ferritins is in one
21 of the amino acids in the coordination environment of site B of the ferroxidase center (Figure 2B). As a
22 consequence, studies of the kinetics of Fe(II) oxidation with various ferritins have resulted in the
23 suggestion of core differences and sometimes mutually inconsistent proposals regarding the mechanism

1 of Fe(II) oxidation in eukaryotic, bacterial, and archaeal ferritins. Some of these differences are listed
2 below and have been discussed in more detail previously¹: (i) measurement of the amount of dioxygen
3 consumed for oxidation of two Fe(II) per ferritin subunit led to the report of differences in eukaryotic and
4 microbial ferritins. For eukaryotic HuHF a stoichiometry of circa 0.45-0.5 O₂ consumed per Fe(II)
5 oxidized has been reported^{47, 48} while for *E.coli* ferritin A (EcFtnA) a stoichiometry of circa 0.35 O₂
6 consumed per Fe(II) oxidized has been observed²¹. These differences have been interpreted in terms of
7 different mechanisms of Fe(II) oxidation in HuHF and PfFtn^{15, 16}. In HuHF it has been proposed that two
8 Fe(II) are simultaneously oxidized but in EcFtnA three Fe(II) are simultaneously oxidized. (ii) It has been
9 observed that the UV-visible absorbance of the peroxodiferric intermediate at 650 nm in human
10 mitochondrial ferritin (MtFtn) is less than that in human H-type ferritin (HuHF)¹⁹. From this observation
11 it has been concluded that in MtFtn less ferroxidase centers are active and that in this ferritin the Fe(III)-
12 mineral core in the internal cavity of protein catalyzes oxidation of Fe(II)¹⁹. (iii) Similar Mössbauer data
13 for bullfrog M ferritin²⁹ (BfMF) and bullfrog H ferritin (BfHF)²⁰ were simulated differently (for detail
14 see reference¹). In BfMF it has been proposed that two Fe(II) are rapidly oxidized in each ferroxidase
15 center via a μ -1,2-peroxodiferric intermediate, which resembles the peroxodiferric intermediate P in
16 soluble methane monooxygenase. Subsequently, the μ -1,2-peroxodiferric intermediate decays slowly to
17 Fe(III) products, which spontaneously move to the core^{17, 18, 29, 42, 43, 49, 50}. However, in bullfrog H-type
18 ferritin (BfHF) it has been proposed that Fe(II) is oxidized via a tyrosine radical intermediate and not a
19 peroxodiferric intermediate^{20, 51}. As a result the Mössbauer spectra collected for BfHF during formation of
20 the intermediates were simulated to show formation of different Fe(III) products instead of the
21 peroxodiferric intermediate²⁰. (iv) Measurement of the progress curves of Fe(II) oxidation for *E.coli*
22 ferritin A (EcFtnA) led to the conclusion that in this ferritin two Fe(II) in the ferroxidase center and an
23 Fe(II) in site C, are oxidized concertedly^{37, 46}. A recent study using EcFtnA led to the conclusion that in
24 this ferritin Fe(II) in site C is oxidized by hydrogen peroxide generated in the ferroxidase center¹⁴. In

1 HuHF using stopped-flow UV-visible spectroscopy progress curves of Fe(III) formation and the
2 peroxodiferric intermediate were measured¹⁷. In contrast to EcFtnA, the data for HuHF were interpreted
3 as oxidation of two Fe(II) in each ferroxidase center observed as a sudden jump in the absorbance
4 between 300-400 nm and the absorbance of the peroxodiferric intermediate at 650 nm. Subsequent
5 gradual increase in the absorbance at 300-400 nm and decrease in the absorbance of the peroxodiferric
6 intermediate at 650 nm was interpreted as release of Fe(III) to the core. Consequently, the UV-visible
7 spectra were simulated using a model to explain Fe(II) oxidation and Fe(III) release. (v) After complete
8 oxidation of Fe(II), Mössbauer measurements were used to study formation of Fe(III) products in
9 different ferritins. The results obtained for EcFtnA⁴⁴ have been interpreted as formation of Fe(III) dimer
10 (circa 60%) and some Fe(III) monomer (circa 30%), while the data obtained for HuHF⁵² have been
11 interpreted as formation of Fe(III) dimer as the main product (circa 70%) and some Fe(III) mineral core
12 (circa 30%). (vi) In bacteria a variant of ferritin, named bacterioferritin, is found, which has a very similar
13 structure to that of ferritin except that it has a heme group between pairs of subunits⁵³ with a role in iron
14 release⁵⁴. While studies with *E.coli* bacterioferritin have led to the conclusion that in bacterioferritins the
15 Fe(III) mineralization process is different from that in eukaryotic and microbial ferritins and proceeds via
16 a diiron cofactor site^{15, 55}, studies with a bacterioferritin isolated from *Desulfovibrio vulgaris*
17 Hildenborough (DvHBfr) have led to the proposal of an Fe(III) mineralization mechanism that is similar
18 to the proposed Fe(III) mineralization process for vertebrate H-type ferritin⁵⁶, the ferroxidase center is a
19 substrate site and not a stable cofactor center. Based on the data and interpretations discussed above the
20 diversity view has emerged: the mechanism of Fe(II) oxidation and storage is different among eukaryotic
21 and microbial ferritins^{15, 22}. For example, , in eukaryotic ferritin two Fe(II) are simultaneously oxidized in
22 each ferroxidase center and in bacterial ferritin three Fe(II) are simultaneously oxidized in the ferroxidase
23 center.

1 In contrast to this diversity view our recent studies using HuHF and Pfftn have led to the emergence of
2 the unifying view of a single mechanism of Fe(II) oxidation and storage by ferritins and bacterioferritins¹.
3 For Pfftn we initially suggested that the Fe(III) in the ferroxidase center is a stable cofactor site⁵⁷ similar
4 to the cofactor site of dioxygen activating enzymes such as soluble methane monooxygenase or similar to
5 the proposed diiron cofactor site in *E. coli* bacterioferritin. Our subsequent studies using HuHF and Pfftn
6 in comparison showed that in Pfftn and HuHF the Fe(III) is not a stable cofactor site⁴. Fe(III) remains
7 metastably in the ferroxidase center. Upon arrival of the new Fe(II) ions, the Fe(III) is sequentially
8 displaced by Fe(II) and moves to the internal cavity⁴. We further observed that although the kinetics of
9 Fe(II) oxidation in HuHF and Pfftn were different¹³, the progress curves of Fe(II) oxidation could be
10 simulated using a common model¹³. Mutagenesis studies of Pfftn compared to those reported for HuHF
11 suggested a role for the highly conserved tyrosine in the vicinity of site B¹³. We proposed that this
12 tyrosine acts as a molecular capacitor for oxidation of Fe(II) in site C via the peroxodiferric intermediate
13 in the ferroxidase center¹³. These data suggested a common mechanism of Fe(II) oxidation and Fe(III)
14 mineralization among eukaryotic and microbial ferritins. To understand the origin of the observed
15 differences in the reported kinetics of Fe(II) oxidation among eukaryotic and microbial ferritins and to
16 check if they reflect different mechanism of Fe(II) oxidation among ferritins we studied and compared the
17 mechanisms of Fe(II) oxidation in HuHF and Pfftn. These two ferritins are from two different Domains
18 of life and should serve as a proper model to test the unity view against the diversity view and to
19 understand differences among eukaryotic and microbial ferritins. We focused on the molecular details of
20 the mechanism of Fe(II) oxidation by dioxygen at three stages of the reaction under single-turnover
21 conditions: binding of Fe(II) ions to sites A, B, and C prior to addition of dioxygen, formation of
22 Fe(II)/Fe(III) intermediates after addition of dioxygen, and finally the appearance of Fe(III) products. The
23 results of anaerobic Fe(II) binding measured by Mössbauer spectroscopy revealed the amount of Fe(II)
24 present in each site, and subsequently the amount of four possible Fe(II)-occupied subunit types (Figure 8

1 and Figure 3): ($A^{II}B^{II}C^0$), ($A^{II}B^{II}C^{II}$), ($A^{II}B^0C^{II}$), and ($A^{II}B^0C^0$) subunits. The major difference between
2 Pfftn and HuHF was the relative amount of each Fe(II)-occupied subunit type. This difference is
3 interpreted to originate from the difference in the affinity of site B in these ferritins for Fe(II) ion.

4 In the next step we analysed the Fe(II)/Fe(III) intermediates during catalysis of Fe(II) oxidation.
5 The Mössbauer parameters that we found for the peroxodiferric intermediate were compared to those
6 reported for different peroxodiferric species in other proteins and model compounds. We observed that
7 the values of the quadrupole splitting (ΔE_Q) in HuHF and Pfftn (Table 3) are not close to those assigned
8 to the μ -1,2-peroxodiferric binding mode in most of the di-iron cofactor enzymes and model compounds.
9 However, the values of the ΔE_Q for the peroxodiferric intermediate in Pfftn and HuHF were close to
10 those reported for the η^2 -O₂ binding mode of dioxygen to Fe(III) in model compounds (Table 3)³⁸.
11 Because EPR spectroscopy showed that the majority of Fe(III) ions are antiferromagnetically coupled we
12 propose a μ - η^1 : η^2 binding mode for the peroxodiferric intermediate in ferritins similar to that proposed
13 for arylamine oxygenase³⁸. For BfMF resonance Raman spectroscopy has been used to determine the
14 molecular structure of the peroxodiferric intermediate. An O-O stretching frequency $\nu(O-O) = 851$ (cm⁻¹)
15 was reported³⁸. The O-O stretching frequencies ($\nu(O-O)$) typically reported for the μ -1,2-peroxodiferric
16 binding mode span a wide range (830-925 cm⁻¹)³⁸ whose minimum is close to the value reported for η^2 -O₂
17 binding mode ($\nu(O-O) = 822$ cm⁻¹)¹. Because a wide range of $\nu(O-O)$ might be expected for different
18 binding modes of the peroxodiferric species, it appears to us that based on the $\nu(O-O)$ alone the exact
19 assignment of the binding mode of the peroxodiferric intermediate in BfMF is not possible and resonance
20 Raman data should be used in combination with Mössbauer data. Because of the available inconsistencies
21 in the reported Mössbauer data for BfMF (Table 3) we cannot conclude that the peroxodiferric
22 intermediate in BfMF has a μ -1,2-peroxo structure. Further experiments using different spectroscopic
23 techniques are required to obtain a better understanding of the molecular structure of the peroxodiferric
24 intermediate in BfMF and other ferritins.

1 Comparison of the Mössbauer data before addition of dioxygen and 0.7 s after addition of dioxygen
2 revealed that only in the ($A^{II}B^{II}C^0$) and ($A^{II}B^{II}C^{II}$) subunits the Fe(II) in sites A and B could be oxidized
3 rapidly to form the peroxodiferric intermediate (Figure 8). Thus, the rapid increase in the absorbance at
4 310 nm in HuHF and Pfftn (Figure 4) is indeed due to formation of the peroxodiferric intermediate and
5 not Fe(III) products. The slower phase of the progress curves of Fe(III) formation at 310 nm (Figure 4),
6 which occurs after 0.7 s, represents the slow oxidation of Fe(II) in site C of the ($A^{II}B^{II}C^{II}$) subunits and
7 that of Fe(II) in ($A^{II}B^0C^0$) and ($A^{II}B^0C^{II}$) subunits. In Pfftn less than 16% of the total Fe(II) added is
8 oxidized slowly and in HuHF circa 37% of the total Fe(II) added is oxidized slowly (Table 2). The
9 difference in the kinetics of Fe(II) oxidation between HuHF and Pfftn originates from the amount of
10 ($A^{II}B^0C^{II}$), ($A^{II}B^0C^0$), and ($A^{II}B^{II}C^{II}$) subunits. In Pfftn the percentages of ($A^{II}B^0C^{II}$) and ($A^{II}B^0C^0$)
11 subunits were negligible and almost all of the Fe(II) in site C was next to fully occupied ferroxidase
12 centers, i.e. ($A^{II}B^{II}C^{II}$) subunits. The Fe(II) in site C of ($A^{II}B^{II}C^{II}$) subunits is proposed to be oxidized
13 presumably by the peroxodiferric intermediate¹³, and in this mechanism the conserved tyrosine provides a
14 fourth electron for complete reduction of molecular oxygen to water¹³. In contrast in HuHF the percentage
15 of ($A^{II}B^{II}C^{II}$) subunits was less than half of that in Pfftn and instead the percentage of ($A^{II}B^0C^{II}$) and
16 ($A^{II}B^0C^0$) subunits together was 25%. The Fe(II) in ($A^{II}B^0C^{II}$) and ($A^{II}B^0C^0$) subunits cannot be oxidized
17 rapidly via the peroxodiferric intermediate. In these subunits the Fe(II) should be oxidized via other
18 mechanisms. A reasonable possibility would be the re-organization of Fe(II) to sites A and B (Figure 8)
19 and subsequent oxidation of Fe(II) via the peroxodiferric intermediate. This is because EPR spectroscopy
20 indicated more than 95% of the Fe(III) to be in antiferromagnetically coupled species. If Fe(II) in site A
21 and site C of the ($A^{II}B^0C^{II}$) and ($A^{II}B^0C^0$) subunits would have been oxidized separately via other
22 mechanisms at least 12% mononuclear Fe(III) should have been observed by EPR, because the Fe(III) in
23 site A cannot spontaneously move to the internal cavity and the Fe(III) ions in site A and C are too far
24 away to be coupled by exchange. The proposal that the Fe(II) ions in ($A^{II}B^0C^{II}$) and ($A^{II}B^0C^0$) subunits

1 first rearranges to sites A and B, for oxidation to occur via the peroxodiferric intermediate is also in line
2 with the previous observations by us ⁴ and others ^{5, 10} that site C in different eukaryotic and microbial
3 ferritins is a transient Fe(II) binding site.

4 In summary, we demonstrated that in Pfftn and HuHF a difference in the occupation of site B
5 with Fe(II) exists, but the same peroxodiferric intermediate forms upon addition of dioxygen, which
6 decays to a major Fe(III)-dimer product. While the exact molecular structure of the peroxodiferric
7 intermediate remains to be determined, the data support the proposal of unity in the biochemistry of
8 ferritins, and they provide a possible explanation for the observed differences among ferritins in the
9 reaction rates, the amount of Fe(II) oxidized per molecular oxygen, and the formation of different Fe(III)
10 products besides the major Fe(III)-dimer. We propose that because of the variation in an amino acid
11 residue of site B, variation in the affinity of this site for Fe(II) among ferritins exists. As a consequence
12 the amount of ($A^{II}B^{II}C^{II}$), ($A^{II}B^{II}C^0$), ($A^{II}B^0C^{II}$), and ($A^{II}B^0C^0$) subunits formed upon addition of Fe(II) will
13 vary. In ferritins with higher percentages of ($A^{II}B^{II}C^{II}$) and ($A^{II}B^{II}C^0$) subunits, more Fe(II) will be
14 oxidized at a fast rate via the peroxodiferric intermediate because Fe(II) in site B is required for catalysis.
15 This will result in different reaction rates as we here observed for HuHF and Pfftn. A higher percentage
16 of ($A^{II}B^{II}C^{II}$) subunits means more Fe(II) will be oxidized in site C together with the Fe(II) in sites A and
17 B to form two water molecules and as a result the amount of Fe(II) oxidized per dioxygen consumed will
18 be different in Pfftn and HuHF as we reported previously¹³. Moreover, differences in the relative number
19 of ($A^{II}B^{II}C^{II}$), ($A^{II}B^{II}C^0$), ($A^{II}B^0C^{II}$), and ($A^{II}B^0C^0$) subunits among ferritins can lead to formation of minor
20 Fe(III) products such as Fe(III)-monomer, Fe(III)-trimer, and Fe(III) mineral core, next to the main
21 Fe(III)-dimer product in the ferroxidase center. The validity of this proposal to other microbial and
22 eukaryotic ferritins remains to be evaluated. It is conceivable that the variation observed in the kinetics of
23 Fe(II) oxidation among ferritins might be relevant to the specific requirement of the iron homeostasis
24 machinery of each organism for managing the intracellular concentrations of free Fe(II) and Fe(III) ions.

1

2 Acknowledgement

3 This work was supported in part by an EMBO Long Term Fellowship (2015-157) to KHE. We thank
4 Marc Strampraad for his assistance with the freeze-quench setup. During the preparation of this work, Dr.
5 Simon de Vries whose work on development of rapid freeze-quench techniques has inspired our present
6 research and who has been a long-time friend, passed away unexpectedly. We dedicate this work to his
7 memory.

8

9 Competing financial interest

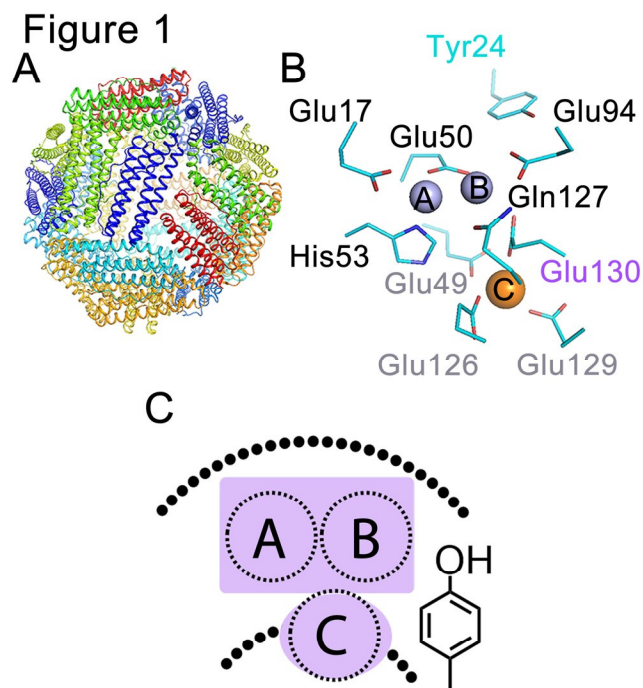
10 The authors declare no competing financial interest.

1 **References.**

- 2 1. K. Honarmand Ebrahimi, P.-L. Hagedoorn and W. R. Hagen, *Chem. Rev.*, 2015, **115**, 295-326.
3 2. G. n. Jutz, P. van Rijn, B. Santos Miranda and A. Böker, *Chem. Rev.*, 2015, **115**, 1653-1701.
4 3. M. Uchida, S. Kang, C. Reichhardt, K. Harlen and T. Douglas, *Biochim. Biophys. Acta*, 2010,
5 **1800**, 834-845.
6 4. K. H. Ebrahimi, E. Bill, P.-L. Hagedoorn and W. R. Hagen, *Nat. Chem. Biol.*, 2012, **8**, 941-948.
7 5. R. K. Behera and E. C. Theil, *Proc. Natl. Acad. Sci.*, 2014, **111**, 7925-7930.
8 6. C. Pozzi, F. Di Pisa, C. Bernacchioni, S. Ciambellotti, P. Turano and S. Mangani, *Acta Cryst.*,
9 2015, **71**, 1909-1920.
10 7. F. Bou-Abdallah, H. Yang, A. Awomolo, B. Cooper, M. Woodhall, S. Andrews and N. Chasteen,
11 *Biochemistry*, 2014, **53**, 483-495.
12 8. A. S. Pereira, C. G. Timóteo, M. r. Guilherme, F. Folgosa, S. G. Naik, A. r. G. Duarte, B. H.
13 Huynh and P. Tavares, *J. Am. Chem. Soc.*, 2012, **134**, 10822-10832.
14 9. K. H. Ebrahimi, P.-L. Hagedoorn and W. R. Hagen, *J. Biol. Chem.*, 2015, **290**, 26801-26810.
15 10. C. Pozzi, F. Di Pisa, D. Lalli, C. Rosa, E. Theil, P. Turano and S. Mangani, *Acta Cryst.*, 2015, **71**,
16 941-953.
17 11. R. K. Watt, R. J. Hilton and D. M. Graff, *Biochim. Biophys. Acta*, 2010, **1800**, 745-759.
18 12. T. Douglas and D. R. Ripoll, *Protein Sci.*, 1998, **7**, 1083-1091.
19 13. K. H. Ebrahimi, P. L. Hagedoorn and W. R. Hagen, *ChemBioChem*, 2013, **14**, 1123-1133.
20 14. N. E. Le Brun, A. Crow, M. E. Murphy, A. G. Mauk and G. R. Moore, *Biochim. Biophys. Acta*,
21 2010, **1800**, 732-744.
22 15. J. M. Bradley, G. R. Moore and N. E. Le Brun, *J. Biol. Inorg. Chem.*, 2014, **19**, 775-785.
23 16. F. Bou-Abdallah, *Biochim. Biophys. Acta*, 2010, **1800**, 719-731.
24 17. F. Bou-Abdallah, G. Zhao, H. R. Mayne, P. Arosio and N. D. Chasteen, *J. Am. Chem. Soc.*, 2005,
25 **127**, 3885-3893.
26 18. G. N. Jameson, W. Jin, C. Krebs, A. S. Perreira, P. Tavares, X. Liu, E. C. Theil and B. H. Huynh,
27 *Biochemistry*, 2002, **41**, 13435-13443.
28 19. F. Bou-Abdallah, P. Santambrogio, S. Levi, P. Arosio and N. D. Chasteen, *J. Mol. Biol.*, 2005,
29 **347**, 543-554.
30 20. A. S. Pereira, P. Tavares, S. G. Lloyd, D. Danger, D. E. Edmondson, E. C. Theil and B. H.
31 Huynh, *Biochemistry*, 1997, **36**, 7917-7927.
32 21. A. Treffry, Z. Zhao, M. A. Quail, J. R. Guest and P. M. Harrison, *FEBS Lett.*, 1998, **432**, 213-
33 218.
34 22. J. M. Bradley, N. E. Le Brun and G. R. Moore, *J. Biol. Inorg. Chem.*, 2016, 1-16.
35 23. R. K. Watt, *ChemBioChem*, 2013, **14**, 415-419.
36 24. W. R. Hagen, *Biomolecular EPR spectroscopy*, CRC press, 2008.
37 25. J. Tatur, W. R. Hagen and P. M. Matias, *J. Biol. Inorg. Chem.*, 2007, **12**, 615-630.
38 26. F. Bou-Abdallah, P. Arosio, P. Santambrogio, X. Yang, C. Janus-Chandler and N. D. Chasteen,
39 *Biochemistry*, 2002, **41**, 11184-11191.
40 27. X. Liu and E. C. Theil, *Proc. Natl. Acad. Sci. USA*, 2004, **101**, 8557-8562.
41 28. A. Treffry, Z. Zhao, M. Quail, J. Guest and P. Harrison, *Biochemistry*, 1995, **34**, 15204-15213.
42 29. A. S. Pereira, W. Small, C. Krebs, P. Tavares, D. E. Edmondson, E. C. Theil and B. H. Huynh,
43 *Biochemistry*, 1998, **37**, 9871-9876.
44 30. K. Honarmand Ebrahimi, P.-L. Hagedoorn and W. R. Hagen, *FEBS Lett.*, 2013, **587**, 220-225.
45 31. T. Ookubo, H. Sugimoto, T. Nagayama, H. Masuda, T. Sato, K. Tanaka, Y. Maeda, H. Okawa, Y.
46 Hayashi and A. Uehara, *J. Am. Chem. Soc.*, 1996, **118**, 701-702.

- 1 32. Y. Dong, Y. Zang, L. Shu, E. C. Wilkinson, L. Que, K. Kauffmann and E. Münck, *J. Am. Chem.*
2 *Soc.*, 1997, **119**, 12683-12684.
- 3 33. K. Kim and S. J. Lippard, *J. Am. Chem. Soc.*, 1996, **118**, 4914-4915.
- 4 34. M. Yamashita, H. Furutachi, T. Tosha, S. Fujinami, W. Saito, Y. Maeda, K. Takahashi, K.
5 Tanaka, T. Kitagawa and M. Suzuki, *J. Am. Chem. Soc.*, 2007, **129**, 2-3.
- 6 35. F. Li, K. K. Meier, M. A. Cranswick, M. Chakrabarti, K. M. Van Heuvelen, E. Münck and L.
7 Que, *J. Am. Chem. Soc.*, 2011, **133**, 7256-7259.
- 8 36. F. A. Chavez, R. Y. Ho, M. Pink, V. G. Young Jr, S. V. Kryatov, E. V. Rybak-Akimova, H.
9 Andres, E. Münck, L. Que Jr and W. B. Tolman, *Angew. Chem.*, 2002, **114**, 157-160.
- 10 37. O. Horner, C. Jeandey, J. L. Oddou, P. Bonville and J. M. Latour, *Eur. J. Inorg. Chem.*, 2002,
11 **2002**, 1186-1189.
- 12 38. T. M. Makris, V. V. Vu, K. K. Meier, A. J. Komor, B. S. Rivard, E. Münck, L. Que and J. D.
13 Lipscomb, *J. Am. Chem. Soc.*, 2015, **137**, 1608-1617.
- 14 39. K. E. Liu, A. M. Valentine, D. Wang, B. H. Huynh, D. E. Edmondson, A. Salifoglou and S. J.
15 Lippard, *J. Am. Chem. Soc.*, 1995, **117**, 10174-10185.
- 16 40. D. Yun, R. García-Serres, B. M. Chicalese, Y. H. An, B. H. Huynh and J. M. Bollinger,
17 *Biochemistry*, 2007, **46**, 1925-1932.
- 18 41. V. V. Vu, J. P. Emerson, M. Martinho, Y. S. Kim, E. Münck, M. H. Park and L. Que, *Proc. Natl.*
19 *Acad. Sci. USA*, 2009, **106**, 14814-14819.
- 20 42. F. Bou-Abdallah, G. Papaefthymiou, D. Scheswohl, S. Stanga, P. Arosio and N. CHASTEEN,
21 *Biochem. J.*, 2002, **364**, 57-63.
- 22 43. J. Hwang, C. Krebs, B. H. Huynh, D. E. Edmondson, E. C. Theil and J. E. Penner-Hahn, *Science*,
23 2000, **287**, 122-125.
- 24 44. E. R. Bauminger, A. Treffry, M. A. Quail, Z. Zhao, I. Nowik and P. M. Harrison, *Biochemistry*,
25 1999, **38**, 7791-7802.
- 26 45. A. Treffry, Z. Zhao, M. A. Quail, J. R. Guest and P. M. Harrison, *Biochemistry*, 1997, **36**, 432-
27 441.
- 28 46. D. M. Kurtz Jr, *Chem. Rev.*, 1990, **90**, 585-606.
- 29 47. G. Zhao, F. Bou-Abdallah, P. Arosio, S. Levi, C. Janus-Chandler and N. D. Chasteen,
30 *Biochemistry*, 2003, **42**, 3142-3150.
- 31 48. B. Xu and N. Chasteen, *J. Biol. Chem.*, 1991, **266**, 19965-19970.
- 32 49. P. Moënné-Loccoz, C. Krebs, K. Herlihy, D. E. Edmondson, E. C. Theil, B. H. Huynh and T. M.
33 Loehr, *Biochemistry*, 1999, **38**, 5290-5295.
- 34 50. J. K. Schwartz, X. S. Liu, T. Tosha, E. C. Theil and E. I. Solomon, *J. Am. Chem. Soc.*, 2008, **130**,
35 9441-9450.
- 36 51. G. S. Waldo and E. C. Theil, *Biochemistry*, 1993, **32**, 13262-13269.
- 37 52. E. Bauminger, P. Harrison, D. Hechel, N. Hodson, I. Nowik, A. Treffry and S. Yewdall,
38 *Biochem. J.*, 1993, **296**, 709-719.
- 39 53. M. A. Carrondo, *EMBO J.*, 2003, **22**, 1959-1968.
- 40 54. H. Yao, Y. Wang, S. Lovell, R. Kumar, A. M. Ruvinsky, K. P. Battaile, I. A. Vakser and M.
41 Rivera, *J. Am. Chem. Soc.*, 2012, **134**, 13470-13481.
- 42 55. Y. Kwak, J. K. Schwartz, V. W. Huang, E. Boice, D. M. Kurtz Jr and E. I. Solomon,
43 *Biochemistry*, 2015, **54**, 7010-7018.
- 44 56. C. G. Timóteo, M. Guilherme, D. Penas, F. Folgosa, P. Tavares and A. S. Pereira, *Biochem. J.*,
45 2012, **446**, 125-133.
- 46 57. K. H. Ebrahimi, P.-L. Hagedoorn, J. A. Jongejan and W. R. Hagen, *J. Biol. Inorg. Chem.*, 2009,
47 **14**, 1265-1274.

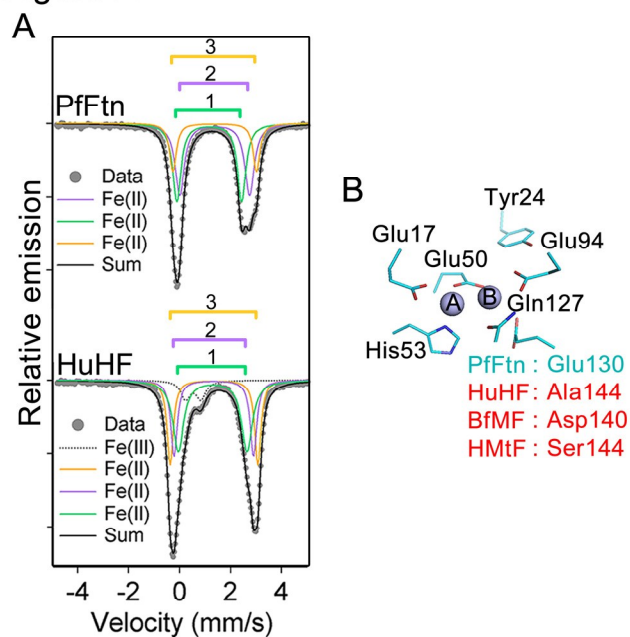
1 Figure legends



2

3 **Figure 1.** Three Fe(II) binding sites exist in ferritins. (A) The conserved nanocage structure of ferritin.
 4 (B) The catalytic center in ferritin consists of two sites, i.e. sites A and B, in the middle of the subunit,
 5 which form the di-iron ferroxidase center, and a third nearby site named site C. The numbering of the
 6 amino acid residues is from *Pyrococcus furiosus* ferritin (Pfftn, PDB 2JD7). An amino acid residue in the
 7 coordination environment of site B and site C that varies among ferritins is numbered in purple. (C) A
 8 cartoon showing the ferroxidase center and site C together with the highly conserved tyrosine in the
 9 vicinity of site B.

Figure 2

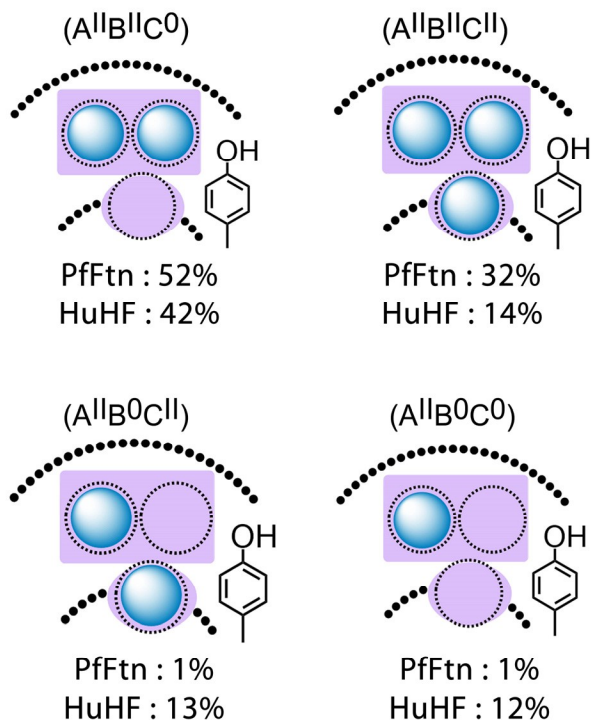


1

2 **Figure 2.** The difference in the coordination environment of site B among ferritins results in differences
 3 in the amounts of four possible Fe(II)-occupied subunit types. (A) Mössbauer spectrum of Fe(II) in PfFtn
 4 and HuHF before addition of dioxygen. In human H-type ferritin (HuHF) a small amount of Fe(III) (less
 5 than 9%) is observed which was due to oxidation of Fe(II) before addition to ferritin. The simulation
 6 results are not biased by this low amount of ‘dirty’ Fe(III). Both in HuHF and PfFtn three distinct Fe(II)
 7 doublets are observed which are assigned to Fe(II) in sites A, B, and C. Measurements were performed at
 8 80 K. (B) Coordination environment of site A is highly conserved and a residue in the coordination
 9 environment of site B, which is also nearby site C, varies among ferritins. The structure shows the amino
 10 acid residues in the coordination environment of the ferroxidase center of PfFtn. The amino acids that are
 11 conserved among ferritins are numbered in black. An amino acid residue in the coordination environment
 12 of site B, which varies among ferritins, is numbered in red. Site C is not shown for clarity.

Figure 3

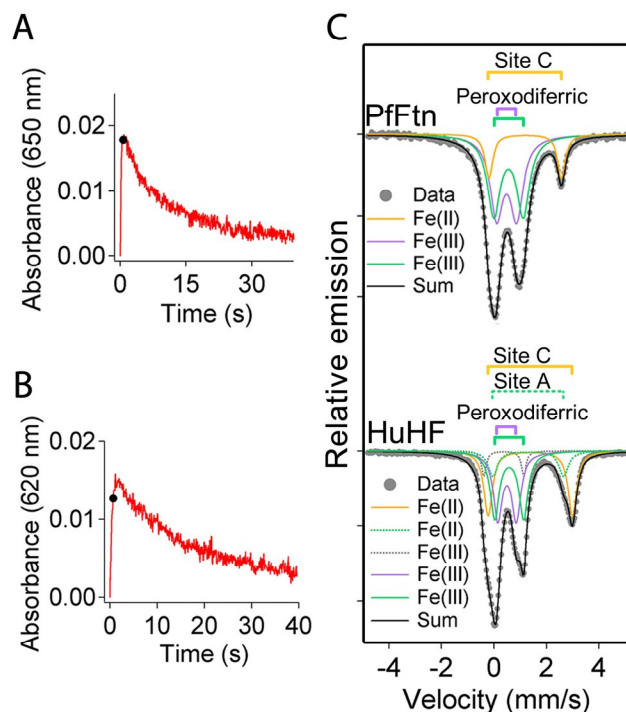
● Fe(II)



1

2 **Figure 3.** The amounts of four Fe(II)-occupied subunit types is different between HuHF and PfFtn. Based
 3 on the results of Mössbauer spectroscopy four possibilities for distribution of Fe(II) among binding sites
 4 exists: subunits with sites A and B filled but site C empty (A^{II}B^{II}C⁰ subunits), subunits with sites A, B,
 5 and C filled (A^{II}B^{II}C^{II} subunits), subunits with sites A and C filled (A^{II}B⁰C^{II} subunits), and subunits with
 6 site A only filled (A^{II}B⁰C⁰ subunits). The percentage of each subunit type varies between HuHF and
 7 PfFtn. The major difference between PfFtn and HuHF is in the percentages of (A^{II}B⁰C^{II}), (A^{II}B⁰C⁰), and
 8 (A^{II}B^{II}C^{II}) subunits. The percentage of (A^{II}B⁰C^{II}) and (A^{II}B⁰C⁰) subunits in PfFtn is negligible.

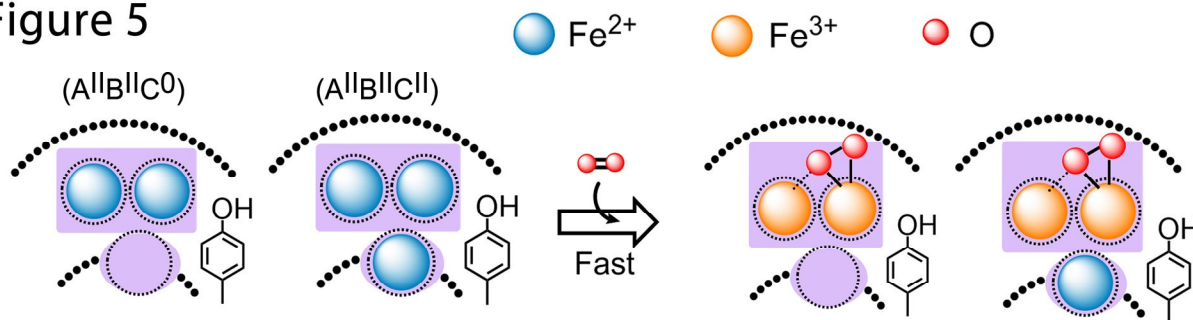
Figure 4



1

2 **Figure 4.** The binding mode of dioxygen in the peroxodiferric intermediate is the same in PfFtn and
 3 HuHF. (A) Progress curves for formation and decay of the peroxodiferric intermediate were recorded at
 4 650 nm for HuHF (2.2 μ M 24-mer) or (B) at 620 nm for PfFtn (4.5 μ M 24-mer). Measurements with
 5 HuHF were performed at 10 $^{\circ}$ C and those with PfFtn were performed at 47 $^{\circ}$ C. (C) Mössbauer spectra of
 6 PfFtn and HuHF 0.7 s after addition of dioxygen. In HuHF besides the two major Fe(III) doublets
 7 attributed to the peroxodiferric intermediate a minor Fe(III) doublet (<6%) was observed (dashed grey
 8 line). The black line (Sum) is the superposition of the simulated subspectra. Measurements were
 9 performed at 80 K.

Figure 5



% of subunits
(A^{II}B^{II}C⁰) (A^{II}B^{II}C^{II})

PfFtn 52 32

1 HuHF 42 14

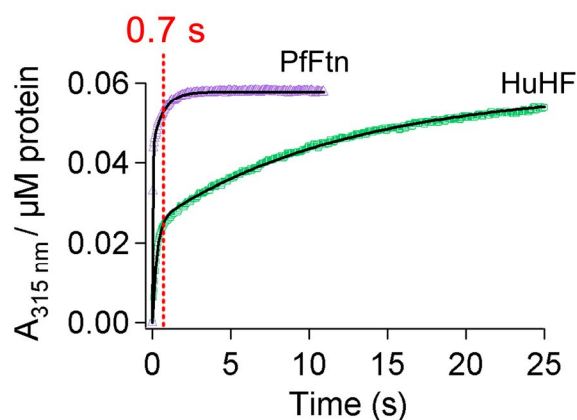
% of subunits

PfFtn 84

HuHF 58

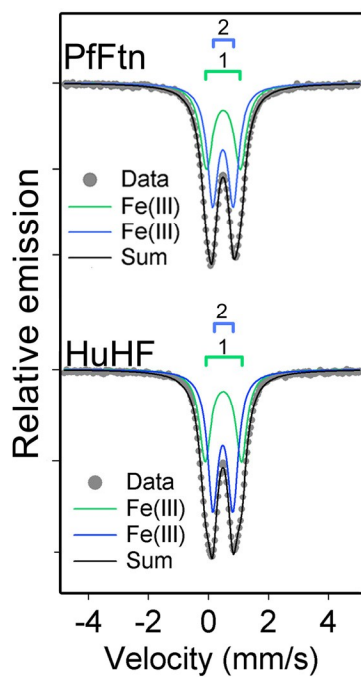
2 **Figure 5.** Under single-turnover conditions two Fe(II) are not simultaneously oxidized in each subunit of
 3 HuHF and PfFtn. A cartoon showing oxidation of Fe(II) in (A^{II}B^{II}C^{II}) and (A^{II}B^{II}C⁰) subunits via the
 4 peroxodiferric intermediate. The total percentage of (A^{II}B^{II}C^{II}) and (A^{II}B^{II}C⁰) subunits observed by
 5 Mössbauer spectroscopy is within experimental error equal to the percentage of the subunits with the
 6 peroxodiferric intermediate. This suggest that only in (A^{II}B^{II}C^{II}) and (A^{II}B^{II}C⁰) subunits two Fe(II) are
 7 simultaneously oxidized in the ferroxidase center to form the peroxodiferric intermediate.

Figure 6



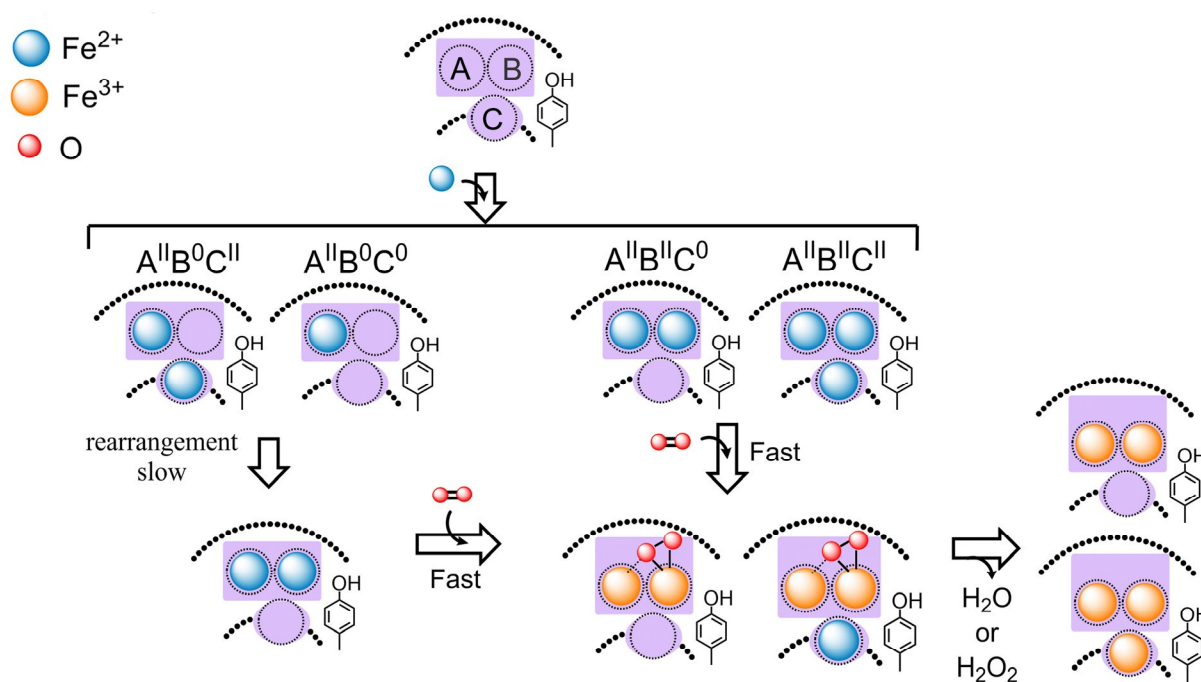
- 1
- 2 **Figure 6.** Stopped-flow UV-visible spectroscopy shows differences in the kinetics of Fe(II) oxidation.
- 3 Progress curves of Fe(III)-species formation were recorded at 315 nm. Circa 2 Fe(II) per ferritin subunit
- 4 were added to PfFtn (4.5 μM 24-mer) or HuHF (2.2 μM 24-mer). Measurements with HuHF were
- 5 performed at 10 $^{\circ}\text{C}$ and those with PfFtn were performed at 47 $^{\circ}\text{C}$. The solid black line shows the fit
- 6 obtained using a two exponential equation (Equation 1). The red dashed line at 0.7 s shows quenching
- 7 time for the Mössbauer measurements in figure 3.

Figure 7



- 1
- 2 **Figure 7.** Fe(III) products in PfFtn and HuHF are the same. Mössbauer spectra of PfFtn and HuHF after
- 3 complete oxidation of Fe(II). Mössbauer spectrum of PfFtn was recorded 300 s after addition of circa 2
- 4 Fe(II) per ferritin subunit and that of HuHF was recorded 60 s after addition of circa 2 Fe(II) per subunit.
- 5 Measurements were performed at 80 K.

Figure 8



1

2 **Figure 8.** A model describing a common mechanism of Fe(II) oxidation for HuHF and PfFtn and the
 3 origin of differences observed in the kinetics of Fe(II) oxidation by these ferritins. Upon addition of Fe(II)
 4 to HuHF and PfFtn different subunit types form: subunits with Fe(II)-occupied sites A and B but empty
 5 site C (A^{II}B^{II}C⁰); subunits with Fe(II)-occupied sites A, B, and C (A^{II}B^{II}C^{II}); subunits with Fe(II)-occupied
 6 site A and C but empty site B (A^{II}B⁰C^{II}); and subunits with Fe(II)-occupied site A only (A^{II}B⁰C⁰). The
 7 Fe(II) in sites A and B of the (A^{II}B^{II}C^{II}) and (A^{II}B^{II}C⁰) subunits is oxidized rapidly via the peroxodiferric
 8 intermediate, which presumably has a μ - η 1: η 2 structure. In these subunits the Fe(II) in site C is possibly
 9 oxidized via the peroxodiferric intermediate in the ferroxidase center as proposed previously¹³. In
 10 (A^{II}B⁰C^{II}) and (A^{II}B⁰C⁰) subunits, whose site B is empty, Fe(II) is first rearranged to fill sites A and B.
 11 The kinetic of this rearrangement process is the rate limiting step in oxidation of Fe(II) in (A^{II}B⁰C^{II}) and
 12 (A^{II}B⁰C⁰) subunits. The model shows a single turnover in the ferroxidase center after addition of Fe(II) to
 13 apo-ferritin, i.e. ferritin with no Fe(III) bound, in the presence of molecular oxygen. For subsequent
 14 turnovers Fe(III) present in the ferroxidase center is displaced by incoming Fe(II).

Tables

Table 1. The amount of Fe(II) in site B and C varies among ferritins.

Protein	Time(s)	Doublet	Oxidation state	Mössbauer Parameters		Site	
				% Fe(II)	δ (mm/s)		ΔE_Q (mm/s)
HuHF	0	1	Fe(II)	39(2)	1.30(2)	2.70(2)	A
		2	Fe(II)	27(1)	1.35(1)	3.44(2)	B and C
		3	Fe(II)	25(1)	1.34(2)	3.12(2)	
Pfftn	0	1	Fe(II)	41(2)	1.38(1)	2.73(2)	A
		2	Fe(II)	40(1)	1.17(1)	2.54(1)	B
		3	Fe(II)	19(1)	1.39(1)	3.27(1)	C

In HuHF at $t=0$ s less than 9% of the $^{57}\text{Fe(II)}$ was observed as Fe(III) (gray line in figure 2a), which we attribute to dirty Fe(III) possibly due to the presence of Fe(III) in Fe(II) solution before addition to HuHF (Supplementary Figure 1). Circa 2 Fe(II) per ferritin subunit were added to Pfftn (45 μM 24-mer) or HuHF (55 μM 24-mer). Measurements were performed under exactly the same conditions. In HuHF Fe(II) is equally distributed among sites B and C and the exact assignment of the second and the third Fe(II) doublet to sites B and C was not possible at this stage.

Table 2. The same peroxodiferric intermediate is formed in Pfftn and HuHF.

Protein	Time(s)	Doublet	Oxidation state	%	Mössbauer Parameters		Site
					δ (mm/s)	ΔE_Q (mm/s)	
HuHF	0.7	1	Fe(III)*	29(1)	0.50(2)	0.70(2)	A and B
		2	Fe(III)*	29(1)	0.58(2)	1.10(2)	
		3	Fe(II)	12(2)	1.32(1)	2.70(2)	A
		4	Fe(II)	25(2)	1.42(2)	3.14(2)	C
Pfftn	0.7	1	Fe(III)*	42(1)	0.49(1)	0.76(1)	A and B
		2	Fe(III)*	42(1)	0.56(2)	1.12(1)	
		3	Fe(II)	16(2)	1.20(1)	2.77(1)	C

Measurements were performed under exactly the same conditions. Circa 2 Fe(II) per ferritin subunit were added. In HuHF a minor Fe(III) doublet (< 6 %) was observed (Figure 3). The Mössbauer parameters of this doublet were different from those of dirty Fe(III) observed in sample before addition of dioxygen: δ (mm/s) = 0.38 (1) and ΔE_Q (mm/s)=1.52 (1). This minor Fe(III) species might be the mononuclear Fe(III) observed by EPR spectroscopy (Supplementary Table 2), whose origin is unknown. * The Fe(III) doublets that form the peroxodiferric intermediate.

Table 3. Comparison of the Mössbauer parameters of the peroxodiferric intermediate in HuHF and PfFtn with those reported for the peroxo species in model compounds and other proteins.

		δ (mm/s)	ΔE_Q (mm/s)	Binding mode of dioxygen	Ref.
PfFtn	Fe(III)	0.49(1)	0.76(1)	$\mu - \eta 1:\eta 2^*$	This work
	Fe(III)	0.56(2)	1.12(1)		
HuHF	Fe(III)	0.50(2)	0.70(2)	$\mu - \eta 1:\eta 2^*$	This work
	Fe(III)	0.58(2)	1.10(2)		
BfMF ^a	Fe(III)	0.62	1.08	---	29
BfMF ^a	Fe(III)	0.65	1.05	---	18
	Fe(III)	0.55	1.06		
MMO	Fe(III)	0.66	1.51	---	39
	Fe(III)				
RNR	Fe(III)	0.63	1.74	μ -1,2-peroxo	40
	Fe(III)				
CmII	Fe(III)	0.61	-0.23 ^b	$\mu - \eta 1:\eta 2$	38
	Fe(III)	0.54	-0.68 ^b		
hDOHH	Fe(III)	0.55	1.16	$(\mu$ -hydroxo) (μ -1,2-peroxo)	41
	Fe(III)	0.58	0.88		
1	Fe(III)	0.58	0.74	Cis- μ -1,2-peroxo	31
	Fe(III)	0.65	1.70		
2	Fe(III)	0.54	1.68	$(\mu$ -oxo) (μ -1,2-peroxo)	32
	Fe(III)				
3	Fe(III)	0.66	1.40	μ -1,2-peroxo	33
	Fe(III)				
4	Fe(III)	0.57	1.44	μ -1,2-peroxo	34
	Fe(III)				
5	Fe(III)	0.58	-0.92	η^2 -O ₂	35
6	Fe(III)	0.52(2)	0.71(2)	η^2 -O ₂	36
	Fe(III)	0.65(2)	1.27(3)		
7	Fe(III)	0.65	0.72	Side-on (η^2 -O ₂)	37

Pyrococcus furiosus ferritin (PfFtn); human H-type ferritin (HuHF); Methane monooxygenase (MMO); ribonucleotide reductase (RNR); Arylamine Oxygenase (CmII); human deoxyhypusine hydroxylase (hDOHH); 1, [Fe₂(Ph-bimp)(C₆H₅COO)(O₂)²⁺]; 2, [[Fe₂O₃(6-Me₃-TPA)₂](ClO₄)₃]⁻; 3, [Fe₂(μ -O₂)(μ -O₂CCH₂Ph)₂(HB(pz')₃)₂]; 4, [Fe₂(LPh₄)-(RCO₂)(O₂)²⁺ (R=Ph₃C (oxy⁻¹))]; 5, [FeIII(TMC)(O₂)⁺]; 6, [Fe₂(O₂)(Ar)₄(py)₂]; 7, [Fe(EDTA)O₂]³⁻. The bonding modes proposed for dioxygen in RNR and complexes 1, 2, 3, 4, and 6 are based on detailed spectroscopic studies. The bonding mode proposed for complex 5 is a suggestion due to the considerable difference between the Mössbauer parameters of this complex and those reported for complexes with μ -1,2-peroxo bonding mode. ^a For BfMF inconsistent Mössbauer parameters have been obtained from simulation of exactly the same Mössbauer spectra. Based on these inconsistent data a μ -1,2-peroxo binding mode has been proposed. ^b Signs unknown. * Postulated.

Table 4. Different kinetic parameters obtained for Fe(II) oxidation in PfFtn and HuHF.

Protein	M	N	T1 (s)	T2 (s)	M_∞
HuHF	0.027 ± 0.001	0.031 ± 0.002	0.27 ± 0.01	12.5 ± 0.1	0.058 ± 0.001
PfFtn	0.045 ± 0.001	0.012 ± 0.001	0.03 ± 0.001	0.7 ± 0.02	0.058 ± 0.001

The kinetic parameters were obtained from a global analysis of the progress curves of Fe(III) formation in figure 6 using equation 10. The M, N, and M_∞ are dimensionless.

Table 5. The same Fe(III) products are formed in the ferroxidase center of PfFtn and HuHF.

Protein	Time(s)	Species	%	Mössbauer Parameters		Site
				δ (mm/s)	ΔE_Q (mm/s)	
HuHF	60	Fe(III)	42(2)	0.49(1)	1.21(2)	A
		Fe(III)	58(1)	0.48(1)	0.67(1)	*B, C, and mineral core
PfFtn	300	Fe(III)	42(2)	0.49(1)	1.14(1)	A
		Fe(III)	58(2)	0.48(1)	0.69(1)	*B, C, and mineral core

Measurements were performed under exactly the same conditions. *Circa 42% of the second Fe(III) doublet in HuHF and PfFtn should be the Fe(III) in site B, because EPR spectroscopy shows negligible amount of Fe(III) monomer. From the remaining amount of the second Fe(III) doublet (circa 16%) some is possibly in site C and is observed as mononuclear Fe(III), and some forms the Fe(III) mineral core.